ARTICLE IN PRESS – Acta Cryst. B

Acta Cryst B
STRUCTURAL SCIENCE
CRYSTAL ENGINEERING
MATERIALS

ISSN 2052-5206

Investigation of the changes in hydrogen bonding accompanying the structural reorganization at 103 K in ammonium iodate

Proof instructions

Proof corrections should be returned by **12 March 2019**. After this period, the Editors reserve the right to publish your article with only the Managing Editor's corrections.

Please
(1) Read these proofs and assess whether any corrections are necessary.
(2) Check that any technical editing queries highlighted in **bold underlined** text have been answered.
(3) Send corrections by e-mail to **actab@iucr.org**. Please describe corrections using plain text, where possible, giving the line numbers indicated in the proof. Please do not make corrections to the pdf file electronically and please do not return the pdf file. If no corrections are required please let us know.

To arrange payment for **open access**, please visit **http://shop.iucr.org/iucrshop/viewitem/openaccess/?code=ra5043**. To purchase printed offprints, please complete the attached order form and return it by e-mail.

Please check the following details for your article

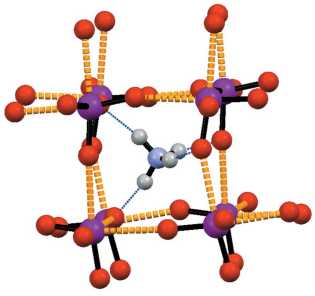

Thumbnail image for contents page

Synopsis: Variable-temperature neutron powder diffraction has been used to study the structure of ammonium iodate from 4.2 K to 290 K, in particular the hydrogen bonding between the ND_4^+ and IO_3^- ions. No phase transition is observed at 103 K, but at low temperatures the ammonium ion is firmly locked in place.

Abbreviated author list: Marshall, W.G. (0000-0003-1727-4609); Jones, R.H. (0000-0003-2907-3118); Knight, K.S. (0000-0003-2395-0407); Pulham, C.R.Smith, R.I.

Keywords: neutron diffraction; hydrogen bonding; phase transitions; variable temperature; ammonium ion

How to cite your article in press

Your article has not yet been assigned page numbers, but may be cited using the doi:

Marshall, W.G., Jones, R.H., Knight, K.S., Pulham, C.R. & Smith, R.I. (2019). *Acta Cryst.* B**75**, https://doi.org/10.1107/S2052520619000325.

You will be sent the full citation when your article is published and also given instructions on how to download an electronic reprint of your article.

Acta Cryst B
STRUCTURAL SCIENCE
CRYSTAL ENGINEERING
MATERIALS
ISSN 2052-5206

Investigation of the changes in hydrogen bonding accompanying the structural reorganization at 103 K in ammonium iodate

W. G. Marshall,[a]‡ R. H. Jones,[b]* K. S. Knight,[a,c,d] C. R. Pulham[e] and R. I. Smith[a]

[a]ISIS Facility, STFC Rutherford Appleton Laboratory, Harwell Campus, Didcot OX11 0QX, UK, [b]School of Chemical and Physical Sciences, Keele University, Keele ST5 5BG, UK, [c]Department of Earth Sciences, University College London, Gower Street, London WC1E 6BT, UK, [d]Department of Earth Sciences, The Natural History Museum, Cromwell Road, London SW7 5BD, UK, and [e]EaStCHEM School of Chemistry, University of Edinburgh, Joseph Black Building, David Brewster Road, Edinburgh EH9 3FJ, UK. *Correspondence e-mail: r.h.jones@keele.ac.uk

Received 20 August 2018
Accepted 7 January 2019

Edited by R. Černý, University of Geneva, Switzerland

‡ 1963–2015

Keywords: neutron diffraction; hydrogen bonding; phase transitions; variable temperature; ammonium ion.

Supporting information: this article has supporting information at journals.iucr.org/b

Neutron powder diffraction has been used to observe the changes in hydrogen bonding that occur as a function of temperature in ND_4IO_3 and, thus, determine the structural features that occur during the low-temperature (103 K) phase transition. It is shown that in the deuterated material the change is not a phase change *per se* but rather a structural reorganization in which the hydrogen bonding becomes firmly locked in at the phase transition temperature, and stays in this configuration upon further cooling to 4.2 K. In addition, both the differences and changes in the axial thermal expansion coefficients in the region 100–290 K can be explained by the changes involving both the hydrogen bonding and the secondary I···O halogen bonds.

1. Introduction

Ammonium iodate has drawn interest because of its pyroelectric (Keve *et al.*, 1971), ferroelectric (Oka *et al.*, 1976), electro-optical (Salje & Bismayer, 1977) and ferroelastic properties (Abdel-Kader *et al.*, 2008) This compound contains both halogen and hydrogen bonds, which may be implicated in these macroscopic properties. In this work, neutron powder diffraction has been used to investigate the changes in halogen and hydrogen bonding that occur as a function of temperature and relate these to some of the macroscopic properties.

The ambient-temperature orthorhombic ($Pc2_1n$) crystal structure of ammonium iodate was first determined over 40 years ago (Keve *et al.*, 1971). It consists of pyramidal IO_3^- anions and tetrahedral NH_4^+ cations [Fig. 1(*a*)]. In addition to the covalent bonds within these ions there are also distinct halogen and hydrogen bonds. In the original structural study, it was not possible to locate the hydrogen atoms, but despite this it was possible to describe the hydrogen bonding within the compound on the basis of the N···O contacts. Two of the oxygen atoms of the IO_3^- group are each involved in one hydrogen bond, whilst the third oxygen atom is implicated in two hydrogen bonds [Fig. 1(*b*)]. In addition to the primary covalent bonds there are also three longer I···O contacts which are much shorter (2.778–2.830 Å) than the sum of the van der Waals radii (3.61 Å) (Rowland & Taylor, 1996). Each of these longer I···O halogen contacts occupies a position which is approximately *trans* to an I—O covalent bond resulting in a highly distorted octahedral environment [Fig. 1(*c*)]. If the coordination of the iodine is considered to be

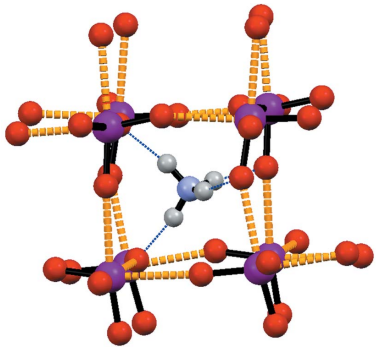

octahedral then the structure has been described as a highly distorted perovskite (Keve *et al.*, 1971) [Fig. 1(*d*)] with the iodine being the sixfold-coordinated atom. The occurrence of these longer I···O contacts and the *trans* geometry found in the O—I···O moieties was commented on by Alcock in his classic review on secondary interactions in inorganic compounds (Alcock, 1972). In this review he listed many interactions which have subsequently been recognized as halogen bonds (Metrangolo *et al.*, 2005). At the time of Alcock's review it was believed that the donor atom in the halogen bond donated a pair of electrons to the σ^* antibonding orbital of the acceptor molecule in line with the then current view of the bonding in charge transfer complexes (Mulliken, 1952). In contrast the current view of bonding in these (halogen-bonded) complexes (which is most widely accepted) focuses on the Coulombic interaction between a region of negative potential situated on the donor and a region of positive potential on the halogen, the so-called σ-hole (Brinck *et al.*, 1992; Politzer & Murray, 2013; Clark *et al.*, 2007). The σ-hole on the halogen lies on the axis which is an extension of the bond between the halogen and the atom to which it is bonded. This model when modified to take account of polarization and dispersion effects (Politzer & Murray, 2013; Politzer *et al.*, 2012) has become the standard description of halogen bonding in the vast majority of such complexes (Cavallo *et al.*, 2016). Complexes involving halogen bonds have not only been investigated because of the basic questions of bonding in these complexes but also because of their role in fields as diverse as supramolecular chemistry (Bertani *et al.*, 2010; Rissanen, 2008), liquid crystals (Nguyen *et al.*, 2004; Cho *et al.*, 2013; McAllister *et al.*, 2013) and biological systems (Auffinger *et al.*, 2004; Scholfield *et al.*, 2013). In biological systems there is also the possibility of the occurrence of additional (C—H···*X*) interactions which may be of importance in controlling the orientation of a substrate molecule at an active site (Lu *et al.*, 2009). We have also shown using neutron powder diffraction that such weak additional hydrogen bond interactions do occur in several simple non-biological systems (Jones *et al.*, 2013, Marshall *et al.*, 2017, 2018) and can be responsible for properties such as colossal thermal expansion (Jones *et al.*, 2014). In NH_4IO_3 there is the possibility of competition between both N—H···O and O—I···O bonds controlling the orientation of the primary IO_3^- units with consequent effects on macroscopic properties.

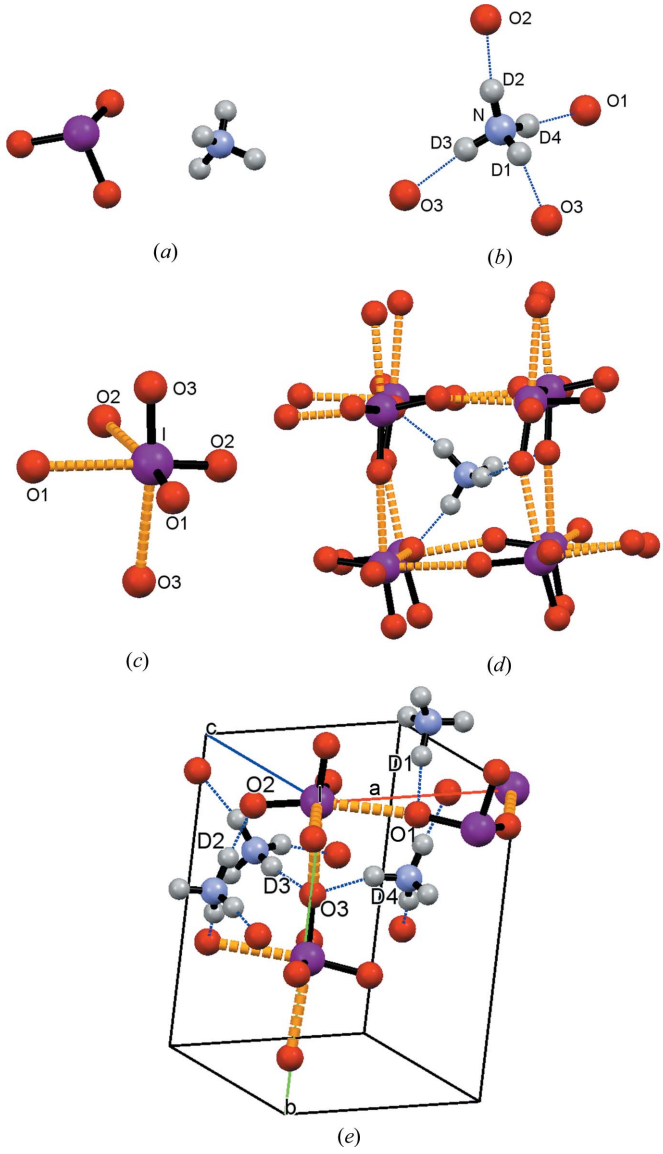

Figure 1
Structures of (*a*) molecular ions, (*b*) hydrogen bonds, (*c*) secondary interactions and (*d*) pseudo-perovskite structure in ND_4IO_3. (*e*) Relationship of molecular ions with respect to the unit cell. Hydrogen bonds are indicated by dotted blue lines, halogen bonds by dashed orange lines.

As we have noted at the outset, ammonium iodate has drawn interest because of its ferroelectric, pyroelectric, electro-optical and ferroelastic properties. One ferroelectric transition is well documented and occurs at 368 K at ambient pressure (Viswanathan & Salje, 1975), for which it was shown that in the immediate pre- and post-transition region there were a series of subtle changes in the structure. In the pre-transition region, it was observed that a contraction occurred along the polar *b* axis. Later work showed that this was accompanied by a simplification of the vibrational spectrum in the N—H region to give a spectrum consistent with a tetrahedral ion in the high-temperature paraelectric phase (Barabash *et al.*, 1999). In the post-transition region there is a further change to give a cubic unit cell at 393 K (Viswanathan & Salje, 1975). A second transition has also been suggested at 103 K (Salje, 1974) and a recent study reporting X-ray diffraction and dielectric permittivity results appears to confirm this (Kader *et al.*, 2013).

Furthermore, it is well known that hydrogen bonding can play a key role in determining the ferroelectric and related properties in both inorganic and organic systems. The prototypical system in the case of inorganic compounds is potassium dihydrogen phosphate (KH_2PO_4) (Busch & Scherrer, 1935), which has been extensively studied, both as a function of temperature and pressure using both X-ray (Endo *et al.*, 1989; Kobayshi *et al.*, 1995; Cai & Katrusiak, 2013) and neutron diffraction (Umebayashi *et al.*, 1967; Tibballs *et al.*, 1982)

techniques. The N—H···O systems have also been extensively studied both in inorganic $NH_4H_2PO_4$ (Lasave *et al.*, 2007; Pérès *et al.*, 1997) and in organic systems (Olejniczak *et al.*, 2013; Zhang *et al.*, 2010), under ambient and non-ambient conditions.

While the structural changes that occur during the high-temperature (368 K) phase transition of ND_4IO_3 have been extensively studied by a wide range of experimental methods (Viswanathan & Salje, 1975; Barabash *et al.*, 1999; Barabash, 1999; Oka *et al.*, 1976; Bergman *et al.*, 1969), much less

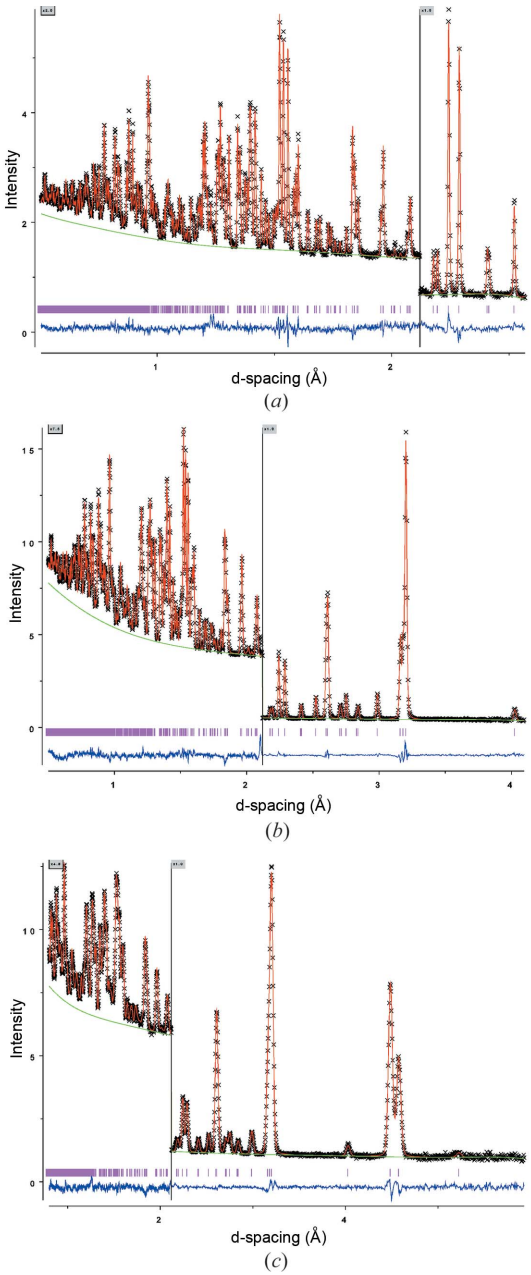

Figure 2
(*a*) Fitted neutron powder diffraction data from ND_4IO_3 at 4.2 K collected in the Polaris backscattering detector bank: (*a*) $\langle 2\theta \rangle$ = 147°, magnified region × 2; (*b*) $\langle 2\theta \rangle$ = 92°, magnified region × 7.5; (*c*) $\langle 2\theta \rangle$ = 52°, magnified region × 4.8. Black crosses = observed data points; red line = calculated fit to data; blue line = difference (obs–calc); green line = calculated background; vertical pink lines = reflection position markers.

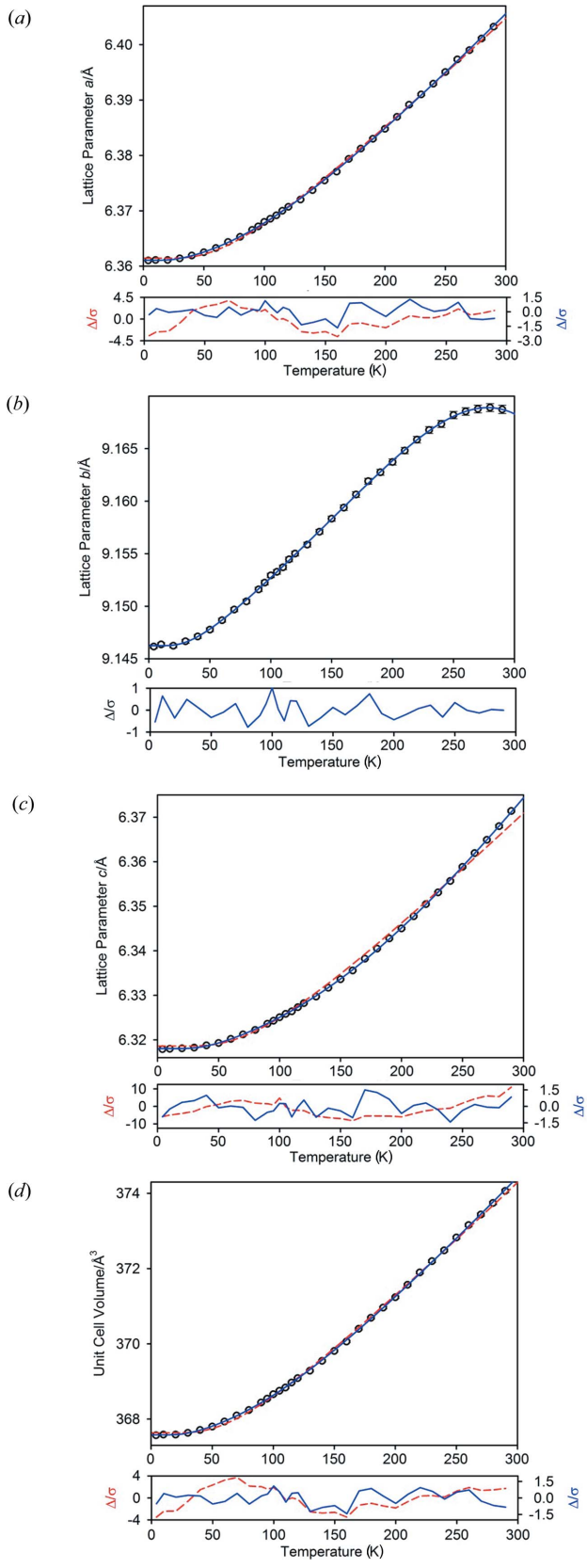

Figure 3
(*a*) Variation in *a* with temperature, (*b*) variation in *b* with temperature, (*c*) variation in *c* with temperature and (*d*) variation in unit-cell volume (*V*) with temperature. In each view the error bars are smaller than the symbols.

attention has been devoted to the low temperature (~103 K transition (Salje, 1974; Kader *et al.*, 2013), though line width studies of the proton NMR spectra indicated that at around 100 K there was a second moment transition (Richards & Schaefer, 1961). It was our aim in this work to establish at an atomic level the nature of the low temperature phase transition, and how this is related to possible changes in both the hydrogen and the halogen bonding within this compound. In order to obtain accurate positions of light atoms (deuterium and oxygen) in the presence of the heavy iodine atoms, we have carried out studies using neutron diffraction on powder samples, making use of the comparable scattering lengths of iodine (b = 5.28 fm), nitrogen (b = 9.36 fm), oxygen (b = 5.803 fm), and deuterium (b = 6.671 fm).

2. Experimental

A sample of deuterated ammonium iodate was prepared by repeatedly exchanging ammonium iodate dissolved in deuterium oxide, followed by removal of solvent using a rotary evaporator attached to a diaphragm pump. Exchange was confirmed by use of infrared spectroscopy and also by the lack of any large incoherent background scattering in the neutron powder diffraction patterns which would have been observed in the presence of any significant quantity of residual hydrogenous material.

Time-of-flight neutron powder diffraction data were collected on the medium-resolution powder diffractometer POLARIS at the ISIS facility Rutherford Appleton Laboratory, UK. Deuterated ammonium iodate was loaded into a 6 mm-diameter thin-walled vanadium sample can which was placed in a helium flow cryostat and data sets collected at 4.2 K (300 μA h proton beam current to the ISIS target, equivalent to ~2 h neutron beamtime) and then from 10 K to 90 K in 10 K steps; 95 K to 120 K in 5 K steps; and 130 K to 290 K in 10 K steps (all for 150 μA h, equivalent to ~1 h). Equilibration times between data sets varied from 6 min (5 K steps) to 10 min (10 K steps). Structure refinement was carried out using the Rietveld method (Rietveld, 1969; van Laar & Schenk, 2018) in space group $Pc2_1n$ [consistent with the non-standard setting of space group $Pna2_1$ used in the original study by Keve *et al.* (1971)] using the *GSAS* (Larson & Von Dreele, 2000) suite of programs through the EXPGUI graphical interface (Toby, 2001). For refinement of the structure at 4.2 K atomic coordinates for the non-hydrogen atoms and unit-cell dimensions were taken from the literature (Keve *et al.*, 1971), and difference Fourier maps calculated in order to locate the deuterium atoms. For each successive higher-temperature data set, starting structural and profile parameters were taken from the results of the previous lower temperature structure refinement. The final fit to the data collected at 4.2 K for selected Polaris detector banks is shown in Fig. 2. The variation of unit-cell parameters is shown in Fig. 3, and selected interatomic contacts and angles as a function of temperature are shown in Fig. 4, and in tabular form in full in the supplementary data. The evolution of the diffraction patterns over the temperature range 90–120 K is given in Fig. 5. Thermal expansion coefficients for the linear

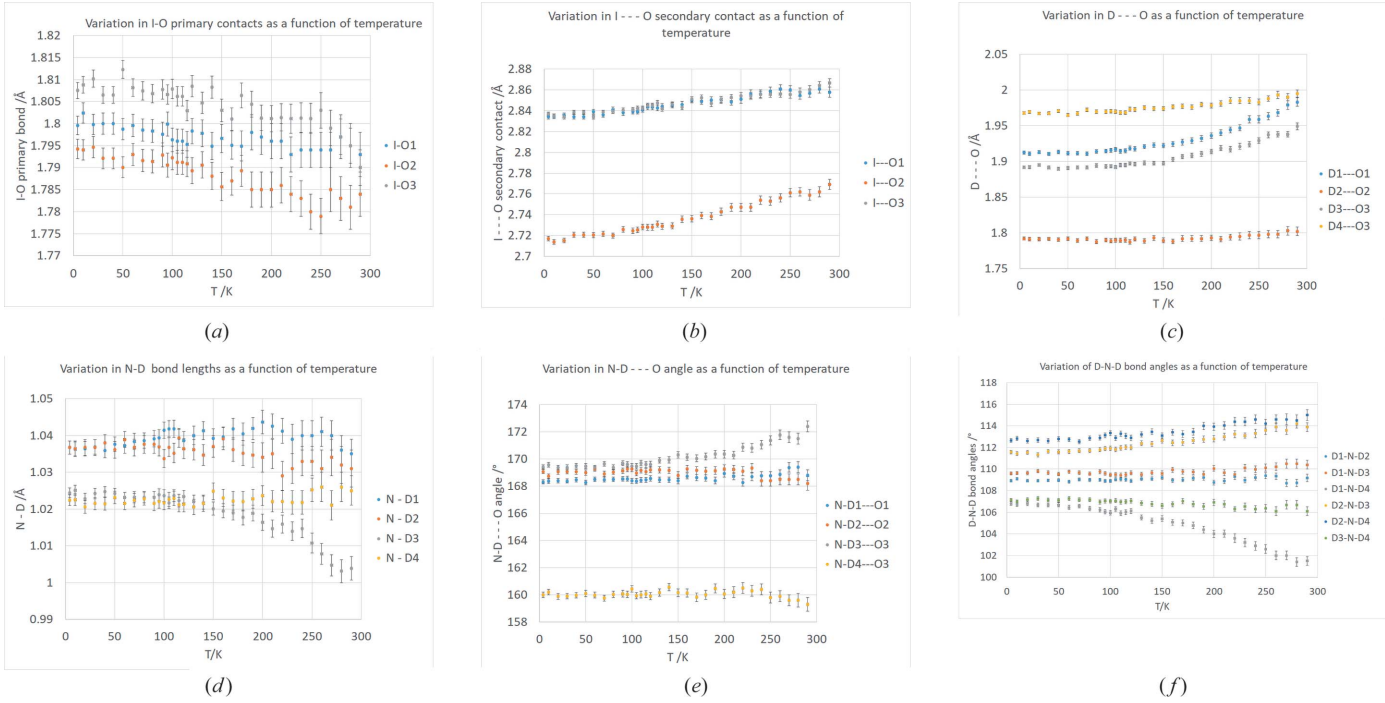

Figure 4
(*a*) Variation in the primary bond lengths in the IO_3^- ion as a function of temperature. (*b*) Variation in the I···O secondary contacts as a function of temperature. (*c*) Variation in D···O as a function of temperature. (*d*) Variation of N—D bonds lengths as a function of temperature. (*e*) Variation in N—D···O angle as a function of temperature. (*f*) Variation of D—N—D bond angles as a function of temperature.

portions of the lattice parameters were calculated used *PAScal* (Cliffe & Goodwin, 2012), and the expansivity indicatrix is shown in Fig. 6.

Examination of the changes in the lattice parameters shows a smooth increase in the *a* and *c* axes as the sample is heated, with the rate of change increasing as the temperature rises. By contrast for the *b* axis, the graph shows a distinct sigmoidal shape, with expansion appearing to stop at about 270 K; with this axis possibly even contracting at temperatures above this.

The data in Fig. 3 shows fits to $a(T) = a_0 + k/[\exp(E/T)-1]$, where a_0 is lattice parameter at 0 K, E is Einstein temperature, k is fitting constant that subsumes the effective bulk modulus and the effective Gruneisen constant (dashed red line in Fig. 3). The effect of modifying this model, by adding an additional term {*i.e* $a(T) = a_0 + k_1/[\exp(E_1/T)-1] + k_2/[\exp(E_2/T)-1]$}, is shown as the full blue lines. The fits assume that the lattice parameters behave in the same way, and for simplicity, the internal energy function is that of an Einstein oscillator (delta function in the phonon density of states). The *b* axis (as commented on previously) is quite clearly different and a single Einstein expression would not fit these data (hence no red line fit). The two-term model, however, fits acceptably well but has $k_2 < 0$ (*i.e* a negative Gruneisen constant) which is clearly necessary to take account of the negative linear thermal expansion. For this to occur at the temperature it does, means that E_2 is very large with respect to E_1. From these fits to the lattice parameters we conclude that these show no obvious premonitory behaviour for the low temperature transition. Further confirmatory evidence for the absence of a gross structural change can be seen in that there are no obvious changes in the diffraction pattern in the range 90–120 K (Fig. 5).

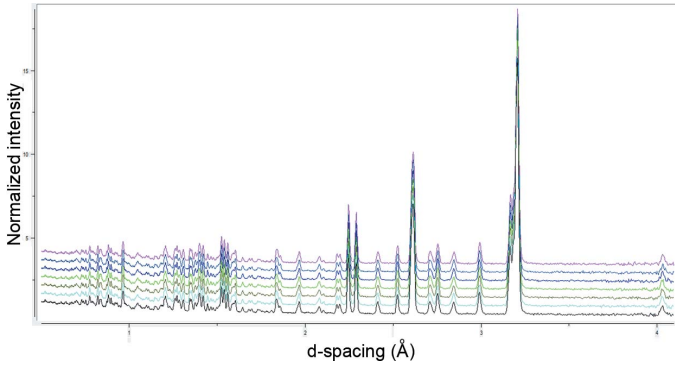

Figure 5
Neutron powder diffraction patterns in the temperature range 90–120 K. Lowest plot is at 90 K.

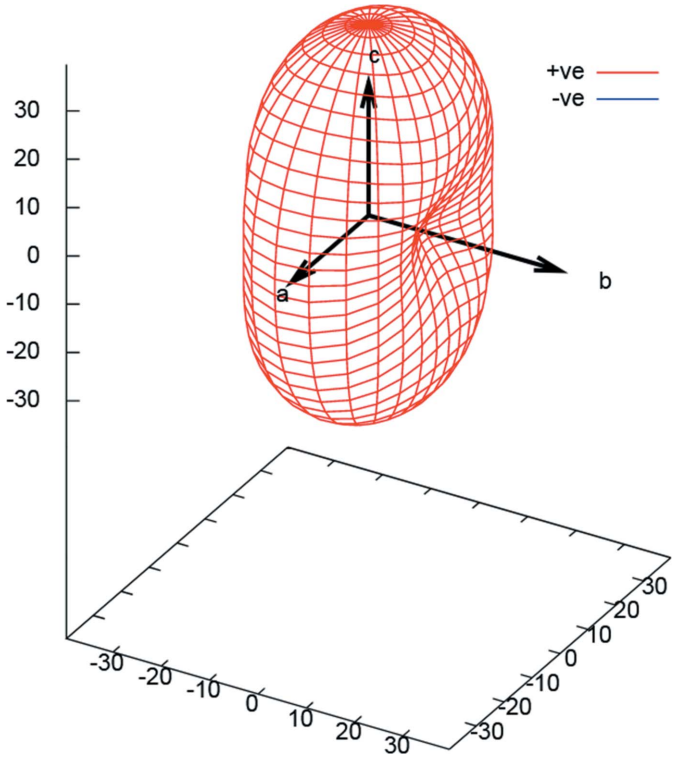

Figure 6
Expansivity indicatrix for linear portion of expansion (150–250 K).

3. Discussion

For the linear portions of the graphs (100–250 K), calculation of the expansion coefficients gives values of $\alpha_a, \alpha_b, \alpha_c$ [30.8 (2), 10.9 (3), 39.6 (6) MK^{-1}]. A contraction of the *b* axis (negative thermal expansion) has been previously reported in the temperature region which precedes the 368 K phase transition (Viswanathan & Salje, 1975). Such a contraction at a ferroelectric transition is not unexpected and has been previously **seen**[34] for example in $PbTiO_3$ and related materials with the perovskite structure (Rossetti *et al.*, 1998; Glazer & Mabud, 1978; Agrawal *et al.*, 1987, 1988), and has been previously commented on in reviews on negative thermal expansion (Evans, 1999), and is associated with the coordination around the sixfold coordinated metal ion becoming more regular. This does not appear to the case in ND_4IO_3 where instead the differences between the primary and secondary contacts in the IO_3^- ion are increasing with temperature, although both the primary and secondary bond lengths become slightly more uniform. The lattice parameters that we determine are in good agreement with those obtained in two of the early studies (Keve *et al.*, 1971; Viswanathan & Salje, 1975). The small differences may be the result of deuteration which is a well known effect in hydrogen-bonded systems (Robertson & Ubbelohde, 1939; Ubbelohde & Woodward, 1942; Jeffrey, 1997), but differ markedly from those obtained in a more recent study (Abdel-Kader *et al.*, 2013), where the lattice parameters reported at 300 K were a = 6.421 (17), 8.875 (8) and 6.251 (6) Å compared with our results at 295 K.

With regard to the interatomic contacts in this compound we will first examine the three hydrogen bonds that are weakest at ambient temperature. As the temperature is raised two of these interactions (N—D1···O1 and N—D3···O3) show a marked increase in the D···O distances above 110 K with one of these D3···O3 being accompanied by increasing linearity of the N—D3···O3 angle. (See comment on lattice parameters mentioned above.) A similar but less pronounced

trend is also observed for the weakest hydrogen bond (N—D4···O3). Finally, it can be seen that the strongest (N—D2···O2) hydrogen bond shows only small changes in the N···O, D···O distances and the N—D···O angle with temperature, implying that the strength of this hydrogen bond does not appreciably change with temperature. Thus it seems likely that the changes previously reported to occur at 103 K are the result of the locking in of the hydrogen bonds below this temperature. These changes in the hydrogen bonding are also seen in the changes in the N—D bond lengths as a function of temperature. Here it can be clearly seen that N—D3 becomes significantly shorter in length as the hydrogen bond in which this atom is involved decreases in strength with increasing temperature. We believe that this is a genuine effect rather than effects associated with libration because the deuterium atoms whose changes in hydrogen bonding are not as dramatic, Figs. 4(*d*), 4(*e*) and 4(*f*) do not appear to show this effect.

The changes caused by temperature on the O—I···O moieties is far less pronounced. Whilst there is a decrease in the primary I—O bond lengths on raising the temperature [Fig. 4(*a*)] it is much smaller than the changes observed in the secondary I···O interactions. There is a small increase in the I···O distances [Fig. 4(*b*)] from about 77.5% to 78.4% of the van der Waals radii. This by itself does not preclude a charge transfer model as the changes in the bond order in such a system are not linear (Bürgi, 1975; Dunitz, 1995). However, a more likely cause of the shortening of the primary covalent bonds at higher temperatures is due to the librational motion of the IO_3^- ions at higher temperatures. Unfortunately, we were unable to obtain reliable anisotropic atomic displacement parameters from the powder diffraction data (unsurprisingly) and thus we were unable to test this hypothesis, which in practice could be determined by a full single crystal analysis.

We have performed a bond valence calculation on the system (Brown & Altermatt, 1985). Whilst the sums at the oxygen atoms (when taking account of additional hydrogen bonding) are plausible, the valence sum at iodine is approximately +5.5, significantly higher than the formal oxidation state of +5. Fig. 7 shows the bond valence sums for the *trans* O—I···O units. The deficiency in the bond valence sum of 2 at oxygen is made up by the contribution of the hydrogen bonds. It can be seen that for all the units there is in general an increase in the bond valence sum with increasing temperature, and what is striking about the graph is that for O3—I···O3 there is a marked increase in the valence sum as the temperature is raised, starting at about 250 K. Looking at Fig. 1(*e*) we see that this unit is aligned almost parallel to **b**. We previously noted that the thermal expansion of **b** starts to decrease rapidly at this temperature and is known in the hydrogenous form to produce negative thermal expansion as the temperature is increased further (Viswanathan & Salje, 1975). Thus the decrease in hydrogen bonding (note O3 is acting as an acceptor to two hydrogen bonds) with increasing temperature leads to incipient regularization of the IO_3 pyramids with concomitant negative thermal expansion in the direction of regularization. This can also be seen by the marked decrease in the I—O3 primary bond length above approximately 250 K [Fig. 4(*a*)]. Further evidence that it is the loss of hydrogen bonding and not regularization of the pyramidal IO_3^- ions in themselves that is responsible for this phenomenon is given by it appearing to start at a lower temperature in the deuterated form that we studied compared to the protonated form (Viswanathan & Salje, 1975), where contraction is known to start no lower in temperature than 293 K. This is because hydrogen bonding involving deuterium was shown to be weaker than that involving hydrogen, in imidazole at around 353 K (Grimison, 1963), and more recently it has been shown (Scheiner & Čuma, 1996) that hydrogen bonds irrespective of their nature (predominantly covalent or ionic) involving deuterium are weaker than those involving hydrogen at higher temperatures. Thus we would expect the loss of hydrogen bonding to occur at a lower temperature for the deuterated compound. Thus from our limited data it appears that the hydrogen bonds are involved in inhibiting regularization of the IO_3^-. A further effect of hydrogen bonding is also seen if we look at the thermal expansion in the *ac* plane. Here it can be seen that the two hydrogen bonds involving O3 lie mainly in a plane approximately parallel to it [Fig. 1(*e*)]. Since the change in hydrogen bonding with temperature is more pronounced for the hydrogen bonds in this plane, and that involving D3 is more pronounced than that for D4, we would expect the expansion to be larger for that involving D3 which is aligned with *c*, followed by that involving D4, which is aligned ∼15° away from a direction, and this is reflected in the magnitudes of α_a, α_b, α_c [30.8 (2), 10.9 (2), 39.6 (6) MK^{-1}].

As we commented on in the *Introduction*, two previous studies on the dielectric properties of these materials have been carried out (Salje, 1974; Abdel-Kader *et al.*, 2013). The earlier study does not permit detailed interpretation as neither dielectric loss data nor the frequency used to determine the permittivity are given, consequently all that can be deduced is that there appears to be a peak in the permittivity at 100 K. The more recent study show a much smaller frequency dependent value for ε'. Frequency dependency was also observed for ε'', with ε'' increasing as the frequency is increased, indicating that there may be a degree of relaxation

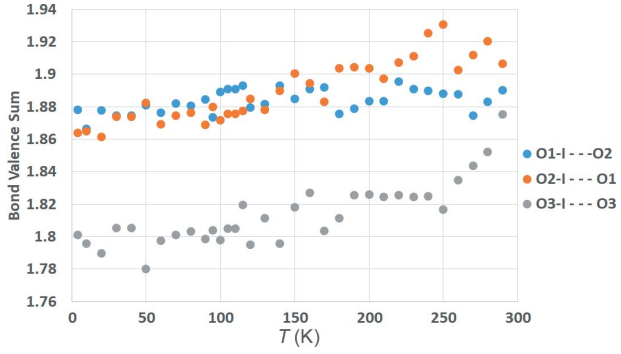

Figure 7
Bond valence sums for *trans* O—I···O moieties versus temperature.

but only at very high frequencies. In addition, the D–E loops do not show any saturation. Taking these results together indicates that the material at low temperature does not display ferroelectricity but rather is a 'lossy' dielectric which may be associated with the reduced motion of the ammonium ions at low temperature. Further evidence for this can be seen in a proton spin relaxation NMR study of this material between 100 and 425 K (Shenoy & Ramakrishna, 1983), which concluded that their results were 'typical of a hindered solid with motions freezing around 77 K'. Our results suggest that this freezing occurs rather at 100 K and is responsible for the observed changes in dielectric behaviour.

4. Conclusion

In conclusion we have established the following points. Firstly the changes in the dielectric properties of the material at 103 K are not the results of a structural phase transition involving either changes in symmetry or large changes in the size of the unit cell, but rather a maximization of the hydrogen bonding on cooling of the three hydrogen bonds that are weakest at room temperature. Secondly the uniaxial contraction of the **b** axis prior to the phase transition at 355 K starts to occur at temperatures below 273 K in the deuterated form and is caused by the reduction in the extent of hydrogen bonding to the oxygen atoms involved in the O—I···O unit which is oriented approximately parallel to this axis. This lower temperature compared to the protonated form is the result of the lower strength of hydrogen bonds involving deuterons compared to protons. Finally, both the magnitude and changes in the magnitude of the thermal expansion coefficients are primarily driven by the changes in hydrogen bonding.

Acknowledgements

We thank the STFC for provision of neutron beam time. We would like to acknowledge helpful advice and comments from Professor Derek Sinclair. We wish to recognize the contribution of the late William George (Bill) Marshall to this project from the conception, execution, and analysis of the data and his contribution to the use of neutron diffraction to the study of hydrogen bonding in condensed matter.

Funding information

The following funding is acknowledged: Science and Technology Facilities Council.

References

Abdel-Kader, M. M., El-Kabbany, F., Naguib, H. & Gamal, W. M. (2008). *Phase Transit.* **81**, 83–99.
Abdel Kader, M. M., El-Kabbany, F., Naguib, H. M. & Gamal, W. M. (2013). *Phase Transit.* **86**, 947–958.
Agrawal, D. K., Halliyal, A. & Belsick, J. (1988). *Mater. Res. Bull.* **23**, 159–164.
Agrawal, D. K., Roy, R. & McKinstry, H. A. (1987). *Mater. Res. Bull.* **22**, 83–88.
Alcock, N. W. (1972). *Adv. Inorg. Chem. Radiochem.* **15**, 1–58.
Auffinger, P., Hays, F. A., Westhof, E. & Ho, P. S. (2004). *Proc. Natl Acad. Sci. USA*, **101**, 16789–16794.
Barabash, A., Gavrilko, T., Eshimov, K., Puchkovskaya, G. & Shanchuk, A. (1999). *J. Mol. Struct.* **511–512**, 145–152.
Barabash, A. I. (1999). *J. Mol. Struct.* **508**, 81–85.
Bergman, J. G., Boyd, G. D., Ashkin, A. & Kurtz, S. R. (1969). *J. Appl. Phys.* **40**, 2860–2863.
Bertani, R., Sgarbossa, P., Venzo, A., Lelj, F., Amati, M., Resnati, G., Pilati, T., Metrangolo, P. & Terraneo, G. (2010). *Coord. Chem. Rev.* **254**, 677–695.
Brinck, T., Murray, J. S. & Politzer, P. (1992). *Int. J. Quantum Chem.* **44**, 57–64.
Brown, I. D. & Altermatt, D. (1985). *Acta Cryst.* B**41**, 244–247.
Bürgi, H. B. (1975). *Angew. Chem. Int. Ed. Engl.* **14**, 460–473.
Busch, G. & Scherrer, P. (1935). *Naturwissenschaften*, **23**, 737–738.
Cai, W. & Katrusiak, A. (2013). *Dalton Trans.* **42**, 863–866.
Cavallo, G., Metrangolo, P., Milani, R., Pilati, T., Priimagi, A., Resnati, G. & Terraneo, G. (2016). *Chem. Rev.* **116**, 2478–2601.
Cho, C. M., Wang, X., Li, J. J., He, C. & Xu, J. (2013). *Liq. Cryst.* **40**, 185–196.
Clark, T., Hennemann, M., Murray, J. S. & Politzer, P. (2007). *J. Mol. Model.* **13**, 291–296.
Cliffe, M. J. & Goodwin, A. L. (2012). *J. Appl. Cryst.* **45**, 1321–1329.
Dunitz, J. D. (1995). *X-ray Analysis and the Structure of Organic Molecules*. 2nd edition. Basel: VCH.
Endo, S., Chino, T., Tsuboi, S. & Koto, K. (1989). *Nature*, **340**, 452–455.
Evans, J. S. O. (1999). *J. Chem. Soc. Dalton Trans.* pp. 3317–3326.
Glazer, A. M. & Mabud, S. A. (1978). *Acta Cryst.* B**34**, 1065–1070.
Grimison, A. (1963). *J. Phys. Chem.* **67**, 962–964.
Jeffrey, G. A. (1997). *An Introduction to Hydrogen Bonding*. New York & Oxford: Oxford University Press.
Jones, R. H., Knight, K. S., Marshall, W. G., Clews, J., Darton, R. J., Pyatt, D., Coles, S. J. & Horton, P. N. (2014). *CrystEngComm*, **16**, 237–243.
Jones, R. H., Knight, K. S., Marshall, W. G., Coles, S. J., Horton, P. N. & Pitak, M. B. (2013). *CrystEngComm*, **15**, 8572–8677.
Keve, E. T., Abrahams, S. C. & Bernstein, J. L. (1971). *J. Chem. Phys.* **54**, 2566.
Kobayashi, Y., Endo, S., Koto, K., Kikegawa, T. & Shimomura, O. (1995). *Phys. Rev. B*, **51**, 9302–9305.
Laar, B. van & Schenk, H. (2018). *Acta Cryst.* A**74**, 88–92.
Larson, A. C. & Von Dreele, R. B. (2000). *General Structure Analysis System* (*GSAS*). Los Alamos National Laboratory Report LAUR 86-748.
Lasave, J., Koval, S., Dalal, N. S. & Migoni, R. L. (2007). *Phys. Rev. Lett.* **98**, 267601.
Lu, Y., Wang, Y., Xu, Z., Yan, X., Luo, X., Jiang, H. & Zhu, W. (2009). *J. Phys. Chem. B*, **113**, 12615–12621.
Marshall, W. G., Jones, R. H. & Knight, K. S. (2018). *CrystEngComm*, **20**, 3246–3250.
Marshall, W. G., Jones, R. H., Knight, K. S., Clews, J., Darton, R. J., Miller, W., Coles, S. J. & Pitak, M. B. (2017). *CrystEngComm*, **19**, 5194–5201.
McAllister, L. J., Präsang, C., Wong, J. P., Thatcher, R. J., Whitwood, A. C., Donnio, B., O'Brien, P., Karadakov, P. B. & Bruce, D. W. (2013). *Chem. Commun.* **49**, 3946–3948.
Metrangolo, P., Neukirch, H., Pilati, T. & Resnati, G. (2005). *Acc. Chem. Res.* **38**, 386–395.
Nguyen, H. L., Horton, P. N., Hursthouse, M. B., Legon, A. C. & Bruce, D. W. (2004). *J. Am. Chem. Soc.* **126**, 16–17.
Mulliken, R. S. (1952). *J. Am. Chem. Soc.* **74**, 811–824.
Oka, T., Mitsui, T., Shiroishi, Y. & Sawada, S. (1976*a*). *J. Phys. Soc. Jpn*, **40**, 913–914.
Olejniczak, A., Anioła, M., Szafrański, M., Budzianowski, A. & Katrusiak, A. (2013). *Cryst. Growth Des.* **13**, 2872–2879.
Pérès, N., Souhassou, M., Wyncke, B., Gavoille, G., Cousson, A. & Paulus, W. (1997). *J. Phys. Condens. Matter*, **9**, 6555–6562.

Politzer, P. & Murray, J. S. (2013). *ChemPhysChem*, **14**, 278–294.
Politzer, P., Riley, K. E., Bulat, F. A. & Murray, J. S. (2012). *Comput. Theor. Chem.* **998**, 2–8.
Richards, R. E. & Schaefer, T. (1961). *Trans. Faraday Soc.* **57**, 210.
Rietveld, H. M. (1969). *J. Appl. Cryst.* **2**, 65–71.
Rissanen, K. (2008). *CrystEngComm*, **10**, 1107–1113.
Robertson, J. M. & Ubbelohde, A. R. (1939). *Proc. R. Soc. A*, **170**, 241–251.
Rossetti, G. A., Cline, J. P. & Navrotsky, A. (1998). *J. Mater. Res.* **13**, 3197–3206.
Rowland, R. S. & Taylor, R. (1996). *J. Phys. Chem.* **100**, 7384–7391.
Salje, E. (1974). *Acta Cryst.* A**30**, 518–521.
Salje, E. & Bismayer, U. (1977). *Opt. Commun.* **20**, 303–304.
Scheiner, S. & Čuma, M. (1996). *J. Am. Chem. Soc.* **118**, 1511–1521.
Scholfield, M. R., Vander Zanden, C. M., Carter, M. & Ho, P. S. (2013). *Protein Sci.* **22**, 139–152.
Shenoy, R. K. & Ramakrishna, J. (1983). *Ferroelectrics*, **48**, 309–312.
Tibballs, J. E., Nelmes, R. J. & McIntyre, G. J. (1982). *J. Phys. C. Solid State Phys.* **15**, 37–58.
Toby, B. H. (2001). *J. Appl. Cryst.* **34**, 210–213.
Ubbelohde, A. R. & Woodward, I. (1942). *Proc. R. Soc. A*, **179**, 399–407.
Umebayashi, H., Frazer, B. C., Shirane, G. & Daniels, W. B. (1967). *Solid State Commun.* **5**, 591–594.
Viswanathan, K. & Salje, E. (1975). *Acta Cryst.* A**31**, 810–813.
Zhang, T., Chen, L., Gou, M., Li, Y., Fu, D. & Xiong, R. (2010). *Cryst. Growth Des.* **10**, 1025–1027.